Basal Dislocation Interactions with a Forest of Non Basal Dislocations in Zinc*

by

N. Nagata+ and T. Vreeland, Jr.
W. M. Keck Laboratories
California Institute of Technology
Pasadena, California

ABSTRACT

The mobility of basal dislocations in 99.999% pure zinc crystals with controlled densities of non basal forest dislocations has been measured as a function of stress at temperatures of 298°K and 84°K. The range of the forest dislocation density was 10^2 to $10^6 cm^{-2}$ and the range of the resolved shear stress was 0 to 34.2×10^6 dyne/cm^2.

The mobility of dislocations was characterized by three distinct regions: a low stress region showing no dislocation motion, a high stress region with a linear velocity-stress relationship, and in between, a transition region, similar to the theoretical predictions. The critical stress for basal edge dislocation motion was found to be proportional to the square root of the forest density and to be temperature independent. A temperature dependent critical stress for basal screw dislocations was observed. A strong interaction between basal dislocations and forest dislocations is indicated. In the high stress region where dislocation velocity is a linear function of the stress the velocity is independent of

---

*This work was supported by the U. S. Atomic Energy Commission.

+Present address: National Research Institute for Metals, Tokyo, Japan.

the forest density. The values of drag coefficient B in this region are in good agreement with those previously reported for specimens with low forest densities (10^2 to $10^3 cm^{-2}$).

INTRODUCTION

Direct measurements of mobility of basal dislocations in zinc (Pope, Vreeland and Wood, 1967; Pope and Vreeland, 1969a) by use of a torsion pulsing technique (Pope, Vreeland and Wood, 1964) have shown that the maximum velocity of dislocation V_{max}, is a linear function of applied shear stress, τ, at stresses above $10^6 dyne/cm^2$ at temperatures ranging from 123^oK to 300^oK and is expressed by

$$BV_{max} = \tau b \qquad (1)$$

where B is a drag coefficient and b is the Burgers vector. The values of B decrease with decreasing temperature. It has been concluded that a dislocation-phonon interaction is responsible for the damping of dislocation motion in an otherwise perfect crystal in zinc.

Velocities less than V_{max} were observed in the direct mobility measurements, and this scatter was tentatively ascribed to interactions with forest dislocations. Flow stress measurements have indicated a strong interaction between basal dislocations and forest dislocations (Stofel and Wood, 1963).

A strong influence of forest dislocations on the flow stress has been reported for close packed metals under the conditions of macroscopic deformation at high rates. Ferguson, Kumar and Dorn (1967), Ferguson, Hauser and Dorn (1967), Victoria, Dharan, Hauser and Dorn (1970), and Kumar and Kimble (1969) found a linear dependence of the flow stress on shear strain rate, expressed as

$$\tau - \tau_B = \alpha \dot{\gamma} \qquad (2)$$

where τ_B is a back stress, α is constant and $\dot{\gamma}$ is the shear strain rate. Since the shear strain rate can be expressed by

$$\dot{\gamma} = \rho_m bV, \tag{3}$$

where ρ_m is the mobile dislocation density and V is the average dislocation velocity, the relation between shear stress and the dislocation velocity can be written as

$$\tau - \tau_B = \alpha \rho_m bV \tag{4}$$

Prestraining was found to increase τ_B and give smaller values of α. These authors considered that τ_B in Eq. (2) was a measure of the stress required to overcome the internal stress field due to forest dislocations. Nagata and Yoshida (1968) have shown that the strain rate of dependence of the flow stress of copper at high strain rates obeys Eq. (2) with $\tau_B = 0$ in crystals with dislocation density at least two order of magnitude lower than those of the aforementioned investigations.

Frost and Ashby (1970) analyzed the viscously damped motion of a dislocation through a regular array of discrete obstacles. Their calculations predicted that, at applied stresses higher than approximately twice the critical stress τ_c necessary to break through the obstacles ($\tau > 2\tau_c$), the motion of the dislocation is essentially governed by the viscous drag and not by the obstacles. In the range $\tau_c < \tau < 2\tau_c$, the average dislocation velocity is influenced by both the viscous drag and the obstacles. Klahn, Mukherjee and Dorn (1970) analyzed the same problem and obtained qualitatively similar results. Existence of a critical stress for dislocation motion through random arrays of obstacles has also been predicted by a statistical

analysis (Kocks, 1966) and by a computer analysis (Foreman and Makin, 1966). Nagata and Vreeland (1970) reported preliminary results on the measurement of the mobility of basal edge dislocations interacting with non basal forest dislocations in zinc at room temperature which qualitatively confirm the theoretical predictions.

The present investigation was undertaken to obtain further quantitative information on how the forest dislocations affect the mobility of both edge and screw oriented basal dislocations in zinc and to compare the results with theoretical predictions.

The tests were conducted on specimens with forest dislocations which were introduced by static compression. Basal dislocations were produced in selected areas by scratching on the basal plane, and these dislocations were displaced by a torsional stress pulse. The basal dislocation configuration before and after testing was observed by means of the Berg-Barrett X-ray technique.

SPECIMEN PREPARATION AND EXPERIMENTAL TECHNIQUES

2.1 Test Specimen Preparation

Randomly oriented single crystals 38mm in diameter were grown from 99.999% pure zinc using the Bridgman Technique. The crystals were cut into rectangular blocks with faces which were parallel to (0001), $\{0\bar{1}10\}$, and $\{2\bar{1}\bar{1}0\}$ by a combination of acid sawing and acid lapping techniques. The (0001) faces which were to serve as the test surfaces were cleaved and the blocks were annealed at 370°C for one hour in an argon atmosphere. The density of non basal forest dislocations at this stage varied between 10^2 and $10^3 cm^{-2}$.

Additional forest dislocations were introduced by compressing the annealed blocks in the $\langle 2\bar{1}\bar{1}0\rangle$ direction. This produced forest dislocations with Burgers vector $\pm(\bar{c} + \bar{a}_1)$ on $(2\bar{1}\bar{1}2)$ planes and $\pm(\bar{c} - \bar{a}_1)$ on $(\bar{2}112)$ planes. The crystallographic relation in this operation is shown in Figure 1. Special care was taken to assure a uniform distribution of load on the compression surface in order to introduce forest dislocations with only Burgers vectors $\bar{c}\pm\bar{a}_1$. Dislocation etch pits after deformation showed a relatively uniform distribution of non basal dislocations in slip bands along $[0\bar{1}10]$, indicating that at most a relatively small number of forest dislocations with $\bar{c}\pm\bar{a}_2$ or $\bar{c}\pm\bar{a}_3$ Burgers vectors were produced. The density of forest dislocations after deformation, as measured by means of the etch pit method, was in the range 10^3 to $2\times10^6 cm^{-2}$.

The deformed blocks were then machined into 12.7mm diameter cylindrical specimens, 5 to 10mm long with [0001] axes. During this operation, the cleaved surfaces were coated with beeswax to prevent acid attack. Most of the specimens were annealed at temperatures above 150^oC for extended periods to reduce the density of forest dislocations to the final test value. Specimens could be retested after removal of the basal dislocations introduced in the test procedure. This removal was accomplished by acid lapping, electrolytic polishing and annealing.

The defect structure of a compressed crystal was examined using transmission electron microscopy. Specimens for this examination were acid cut from the (0001) surfaces of the crystal and electrolytically thinned. The majority of the defects seen were isolated basal and second order pyramidal dislocations. Because of the relatively large dislocation

spacings at 20,000X, densities were not measured. They were, however, in order of magnitude agreement with the etch pit and X-ray observations.

2.2 Method of Producing Basal Dislocations

Fresh basal dislocations were introduced by scratching the basal plane surface of each test specimen with an Al_2O_3 whisker. The load ranged from 75mg (low forest density crystals) to 225 mg. Most of the test specimens were scratched along three $<0\bar{1}10>$ diameters to introduce pure edge dislocations as seen in Figure 1. These scratches served for tests on the displacements of basal edge dislocations. The mobility of screw oriented dislocations was studied by employing a series of short scratches, 0.4mm long, along $<0\bar{1}10>$ directions. Dislocation segments near the tips of these scratches were perpendicular to $<0\bar{1}10>$ directions and were therefore in a pure screw orientation.

2.3 X-Ray Technique and Loading System

Dislocation configurations near the test surface of the specimen were determined before and after tests by the Berg-Barrett X-ray technique. Topographs of the specimen were made using CrKα radiation reflecting from $\{0\bar{1}13\}$ planes.

The scratched surface of the specimen was bonded to a torsion testing machine. Quartz type sticky wax was used for room temperature tests, and bonding agents developed by Gorman, Wood and Vreeland (1969) and Jassby and Vreeland (1970) were employed for tests at 84°K.

A torsion pulse was applied to the specimen by using a torsion testing machine as described by Pope, Vreeland and Wood (1964, 1967).

Pulse durations ranged from 30μsec to 100μsec, and resolved shear stress ranged from 0 to 34.2x10^{6}dyne/cm^2. A typical example of a torsional stress pulse is shown in Figure 2. The time between scratching and loading was usually less than one hour. Dislocation displacements were determined by comparing the Berg-Barrett topographs taken before and after the pulses were applied (Turner, Vreeland and Pope, 1968).

After taking Berg-Barrett topographs, specimens were etched for 6 to 12 sec at -60° to -70°C in a solution of 30ml ethanol, 1ml hydrobromic acid and 1ml bromine. The etch reveals dislocation intersections on (0001) surfaces.

EXPERIMENTAL RESULTS

3.1 Dislocation Displacements

Since the specimen is loaded in torsion, the shear stress on a basal plane is a linear function of radius given by

$$\tau = \tau_{max}(r/R), \qquad (5)$$

where τ_{max} is the stress at the maximum radius, R, and r is the distance from the specimen center.

Figure 3 shows Berg-Barrett photographs of the dislocation configuration around long scratches taken before and after testing. Figure 3(a) shows edge dislocations produced in a crystal with a forest dislocation density of the order of 10^5cm^{-2}. Average spacing of the basal dislocations ranges from 6×10^{-4}cm to 3×10^{-4}cm in different regions adjacent to the scratch. Figure 3(b) is an example of the edge dislocation displacements for specimens with low forest dislocation densities (10^2cm^{-2}). It is seen that the dislocation

displacements are a linear function of radius, even very near the center of the specimen. The stress pulse was essentially rectangular as seen in Figure 2, so the velocity is given by the dislocation displacement divided by the pulse duration. This fact, and the linear stress versus radius relationship means that the experimental curve of displacement versus radius has the same shape as the velocity versus stress curve.

Therefore, it is clear that the dislocation velocity is a linear function of stress for stresses much less than τ_{max} in specimens with a low forest density. Figure 3(c) is an example of edge dislocation displacements at room temperature for specimens with high forest dislocation densities. In contrast with Figure 3(b), dislocation displacements are not linear with radius. Figure 4 is the maximum displacement versus radius plot obtained from Figure 3(c). The envelope of the dislocation displacement is quite similar to that predicted by Frost and Ashby (1970), and Klahn, et al. (1970). The dislocation displacements can be divided into three distinct regions, i. e., a low stress region showing no dislocation displacement, a high stress region with a linear displacement with radius and in between, a transition region. Also, Figure 3(c) and Figure 4 clearly reveal the existence of a critical shear stress for the motion of dislocations. These three regions were found at all temperatures in specimens with forest dislocation densities above $10^4 cm^{-2}$.

Figure 5 shows a Berg-Barrett picture of a specimen with short scratches and a forest dislocation density of $6x10^4 cm^{-2}$, tested at room temperature. Pure screw components can be observed on the segments of curved dislocations (perpendicular to the scratches). Figure 6 is the

displacement versus radius plot obtained from Figure 5. The screw dislocation displacements were obtained by measuring the distance between the tip of each scratch and the screw component of the farthest dislocations in the direction perpendicular to its Burgers vector.

3.2 Critical Stress

Table 1 lists values of the critical stress, τ_c, for edge dislocations at room temperature. These values were determined using the radius at which dislocations started to move, and the known value of τ_{max} in Eq. 1. The corresponding forest density was determined from an etch pit count in an area of the order of $10^{-4}cm^2$ adjacent to the point along the scratch where dislocations started to move. Table 2 compares values of τ_c for edge dislocations from tests at different temperatures. There is no significant variation of the critical stress with temperature.

The critical stress for screw oriented dislocations is more difficult to determine because they could not be introduced in long, continuous segments. The ends of the short scratches were radially spaced by about R/35, and this introduced an uncertainty in the critical stress of about $\tau_{max}/35$ which was less than $4x10^5 dynes/cm^2$ for all tests.

The critical stress for screw oriented dislocations at 298^oK and 84^oK is given in Table 2. Values at 298^oK are below those for edge dislocations, but the difference is within the experimental uncertainty. In contrast to the results for edge dislocations, the critical stress measured for screw dislocations at 84^oK is greater than the 298^oK value.

3.3 Dislocation Drag Coefficient

In the high stress region the maximum displacements are a linear function of radius as seen in Figures 4 and 6. This implies that Eq. 1 is obeyed in the high stress region even for specimens with high forest dislocation densities. The drag coefficient is

$$B = \frac{\tau_{max} bt}{R} \cot\theta \qquad (6)$$

where t is the duration of the stress pulse and $\tan\theta$ is the slope of the displacement versus radius plot. Experimental values of B are listed in Table 3. The values of B for specimens with low forest dislocation densities obtained in previous investigations are listed for comparison. Good agreement is found between the various measurements.

DISCUSSION

4.1 The Effect of Long Range Dislocation Interactions

Scratching introduces a number of nearly parallel dislocations whose interactions can be shown to be negligible. Their spacing before application of the stress pulse is about 4μ, and dislocations at this spacing and far removed from the free surface would interact significantly. However, since the dislocations are within about 2.5μ of the free (0001) surface (Pope and Vreeland, 1969b) the interaction stresses are negligible compared to the applied stress. Forest dislocations spacings were large compared to 2.5μ, so their long range stress fields do not produce a glide force on the basal dislocations which are near the free surface. The forest dislocations therefore act as discrete obstacles to basal dislocations, and

only short range interactions are important.

4.2 Short Range Interactions with the Forest

Saada (1962) treated reactions between gliding dislocations and forest dislocations in the FCC structure. His analysis distinguishes two cases, one in which the gliding dislocation is attracted to the forest dislocation, and one in which it is repulsed. It is more difficult for the gliding dislocation to cut across an attractive forest than a repulsive one, and the stress required to cut through an attractive forest is practically temperature independent while this stress is temperature dependent for a repulsive forest. Quantitative theoretical treatments of the short range dislocation interactions which take place in the present experiments have not yet been made. A quantitative measure of some of the various interactions will be obtained by analysing the experimental results and using theoretical predictions of the relative strengths of the various interactions.

Forest dislocations which have sufficient edge component will in some cases react with basal dislocations to form attractive junctions. The attractive interaction, $\bar{a}_1 + (\bar{c}-\bar{a}_1) \rightarrow \bar{c}$ and $\bar{a}_1 - (\bar{c}+\bar{a}_1) \rightarrow -\bar{c}$, is stronger than the repulsive interaction, $\bar{a}_1 + (\bar{c}+\bar{a}_1)$ and $\bar{a}_1 - (\bar{c}-\bar{a}_1)$, according to an analysis similar to that used by Saada. The uniform a_1 axis compression should produce the same number of positive and negative dislocations on the $(2\bar{1}\bar{1}2)$ and the $(\bar{2}112)$ slip planes. Thus, half of the forest may have attractive interactions with $\bar{a}_1$ basal dislocations and half repulsive, resulting in an effective density, $\rho = \rho_f/2$ for each where ρ_f is the total density of forest dislocations. Two different interactions

between forest dislocations and $\bar{a}_2$ or $\bar{a}_3$ basal dislocations are possible, and typical examples are

$$\bar{a}_2 + (\bar{c}+\bar{a}_1) \rightarrow \bar{c}-\bar{a}_3 \qquad (a_2 \text{ attractive})$$

and

$$\bar{a}_2 + (\bar{c}-\bar{a}_1) \qquad (a_2 \text{ repulsive})$$

The effective forest density is $\rho = \rho_f/2$ for each of these reactions. Again, the strength of the attractive interaction will be greater than that of the repulsive interaction, while both will be weaker than the a_1 attractive interaction.

4.3 The Strength of the Short Range Interactions

The strength of some of the interactions can be deduced from the critical stress measurements using the effective line energy E, of the basal dislocations and the density and distribution of the forest dislocations. The appropriate line energy is that for the basal dislocation in the critical configuration.

As discussed above, the nearly free surface effectively cancels long range dislocation interactions so that the line energy depends only upon the local dislocation configuration around the obstacle. The appropriate line energy has been determined (Nagata, Jassby and Vreeland, 1971) by measurement of the Frank-Reed stress for unstable growth of pinned edge dislocations of known length, which is given by

$$\tau_c = \frac{2E_{screw}}{bl} \qquad (7)$$

where l is the distance between the pinned ends. This determination gave $E_{screw} = 2.9 \times 10^{-4}$ dynes for a dislocation in the screw orientation,

and $E_{edge} = 3.3 \times 10^{-4}$ dynes was deduced using the experimental value for E_{screw} and the ratio of line energy of edge and screw dislocations calculated from anisotropic elasticity theory. These values of line energy are used in the following calculations, and this implies no interaction between the basal dislocation segments which bow around a forest dislocation. Neglect of this interaction causes the line energy to be overestimated resulting in a lower bound estimate for the obstacle strength when it is determined from the measured values of critical stress.

Kocks (1966) and Foreman and Makin (1966) have considered the critical stress for the motion of a dislocation through a random array of strong, discrete obstacles that cannot be sheared but must be passed by dislocation bowing. Their results predict a critical stress of the form

$$\tau_c = \beta \frac{2E}{b} \sqrt{\rho} \qquad (8)$$

where $\beta = 0.84$ (Kocks, approximate value from a statistical study), or

$= 0.81$ (Foreman and Makin from a computer study), and

ρ = obstacle density

The term $\sqrt{\rho}$ may be interpreted as the reciprocal of a uniform obstacle spacing that would give the same critical stress as the random array. Groups of closely spaced obstacles in the random array are bypassed by the gliding dislocation leaving a dislocation surrounding each of these groups. The effective spacing of obstacles is then greater than the average spacing, so that the value of β is less than unity. The majority of scatter in the critical stress values observed in this investigation can be attributed

to variations in the distribution of the forest dislocations since we expect values of β to fall between 0.8 and 1.0.

When the obstacles are somewhat weaker, they may be sheared, and the critical stress may be written as

$$\tau_c = \beta k \frac{2E}{b} \sqrt{\rho} \qquad (9)$$

where k is a constant ($k<1$) characteristic of the strength of the dislocation-obstacle interaction. As stated above, k values for the attractive forest should be larger than those for the repulsive forest. The observation that the critical stress for edge basal dislocations is independent of temperature indicates that the attractive reactions are more important than the temperature dependent repulsive reactions. Values of βk for these reactions may be calculated from the equation

$$\tau_c = \beta k \frac{2E}{b} \sqrt{\rho_f/2} \qquad (10)$$

and are given in Table I. Average calculated values, using a line energy of 3.1×10^{-4} dynes for a mixed dislocation, are

$$\beta k_{a1} = 0.56$$

and

$$\beta k_{a2} = 0.43$$

Taking $\beta = 0.84$ for a random array gives

$$k_{a1} = 0.67$$

and

$$k_{a2} = 0.51$$

These values indicate critical bowing angles of 46° and 34° respectively where 90° is the critical angle for the ideally strong obstacle (Nagata, et al., 1971).

The apparent temperature dependence of the critical stress for basal screw dislocations may arise from the additional drag due to the

sessile jogs which are created when the forest dislocations are cut. A significant reduction in mobility of the basal dislocations (due to jog drag) would require the use of significantly longer pulse durations to determine the actual critical stress. The jogs do not affect the mobility of the basal screw dislocations at high stresses, since the experimental values of B_{screw} are independent of forest density.

ACKNOWLEDGEMENTS

The authors are indebted to Mr. A. Illig for his patience and care in the preparation of specimens. They also wish to thank Dr. K. Jassby for helpful discussions and Prof. R. E. Villagrana for assistance with the electron microscopy. N. Nagata gratefully acknowledges the National Research Institute for Metals for the leave of absence which made possible his stay in the United States.

REFERENCES

Ferguson, W. G., Kumar, A., and Dorn, J. E., 1967, J. Appl. Phys., 38, 1863.

Ferguson, W. G., Hauser, F. E., and Dorn, J. E., 1967, Brit. J. Appl. Phys., 18, 411.

Foreman, A. J. E., and Makin, M. J., 1966, Phil. Mag., 14, 911.

Frost, H. J., and Ashby, M. F., 1970, Tech. Report No. 1, O.N.R. Contract N00014-67-A-0298-0020.

Gorman, J. A., Wood, D. S., and Vreeland, T., Jr., 1969, J. Appl. Phys., 40, 903.

Jassby, K. M., and Vreeland, T., Jr., 1970, Phil. Mag., 21, 1147.

Klahn, D., Mukherjee, A. K., and Dorn, J. E., 1970, Proc. 2nd Int'l Conf. on Strength of Metals and Alloys (A.S.M.), 951.

Kocks, U. F., 1966, Phil. Mag., 13, 541.

Kumar, A., and Kimble, R. G., 1969, 40, 3475.

Li, J. C. M., 1968, Dislocation Dynamics, (New York: McGraw-Hill), p. 87.

Nagata, N., Jassby, K. M., and Vreeland, T., Jr., to be submitted to Phil. Mag.

Nagata, N., and Yoshida, S., 1968, J. Japan Inst. Metals, 32, 3851 (in Japanese).

Nagata, N., and Vreeland, T., Jr., 1970, Proc. 2nd Int'l Conf. on Strength of Metals and Alloys (A.S.M.), 423.

Pope, D. P., and Vreeland, T., Jr., 1969a, Phil. Mag., 20, 1163.

Pope, D. P., and Vreeland, T., Jr., 1969b, Trans. AIME, 245, 2447.

Pope, D. P., Vreeland, T., Jr., and Wood, D. S., 1964, Rev. Scient. Instrum., 35, 1351.

Pope, D. P., Vreeland, T., Jr., and Wood, D. S., 1967, J. Appl. Phys., 38, 4011.

Saada, G., 1962, Electron Microscopy and Strength of Crystals (New York: Interscience Publishers), p. 651.

Stofel, E. J., and Wood, D. S., 1963, Fracture of Solids, (New York: Interscience Publishers), p. 521.

Turner, A. P. L., and Vreeland, T., Jr., and Pope, D. P., 1968, Acta Cryst., A24, A52.

Victoria, M. P., Dharan, C. K. H., Hauser, F. E., and Dorn, J. E., 1970, J. Appl., Phys., 41, 674.

Vreeland, T., Jr., and Jassby, K. M., 1971, Mater. Sci. Eng., 7, 95.

FIGURE 1

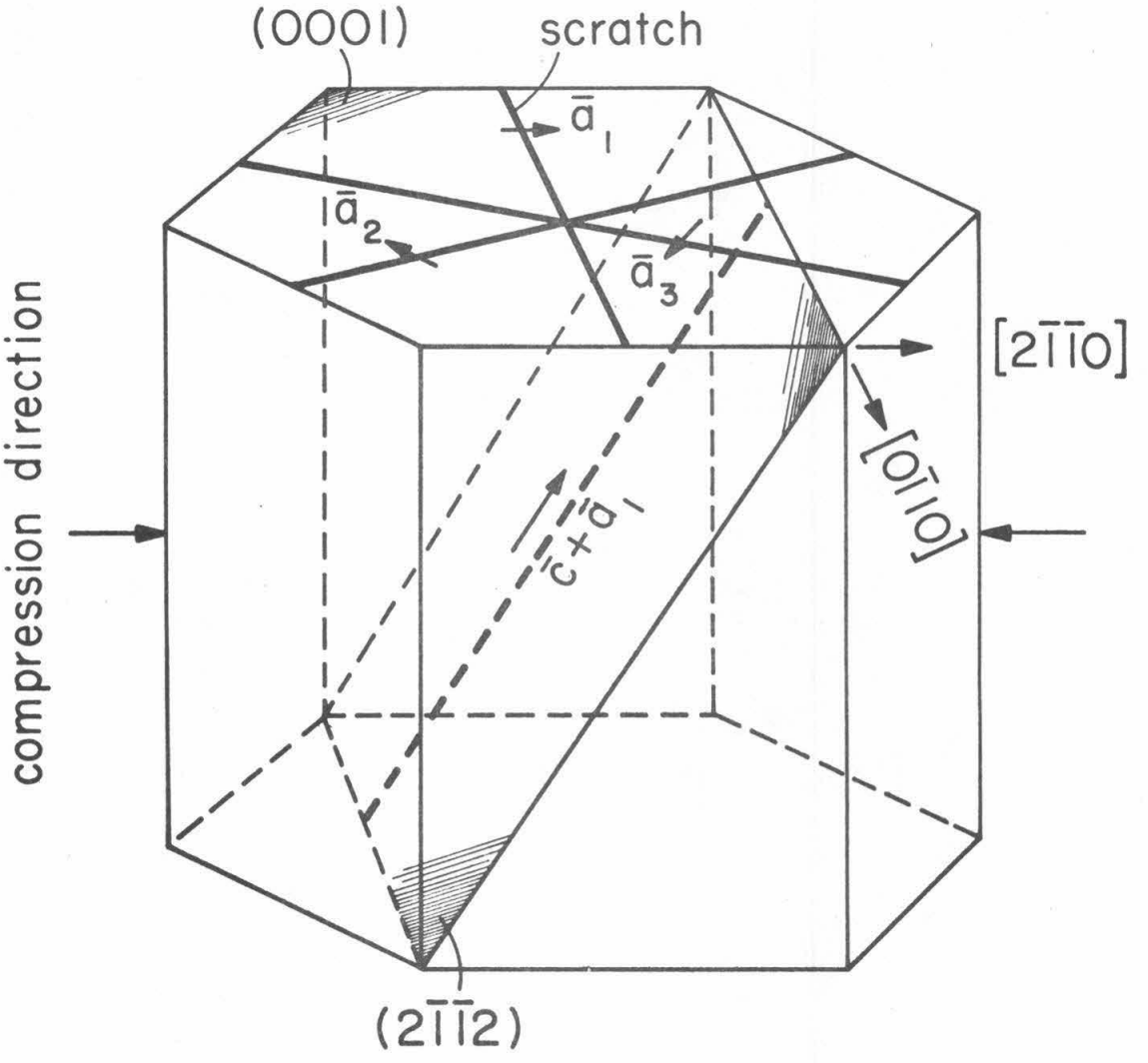

Schematic diagram indicating the scratches and basal and non basal dislocations in a test specimen.

FIGURE 2

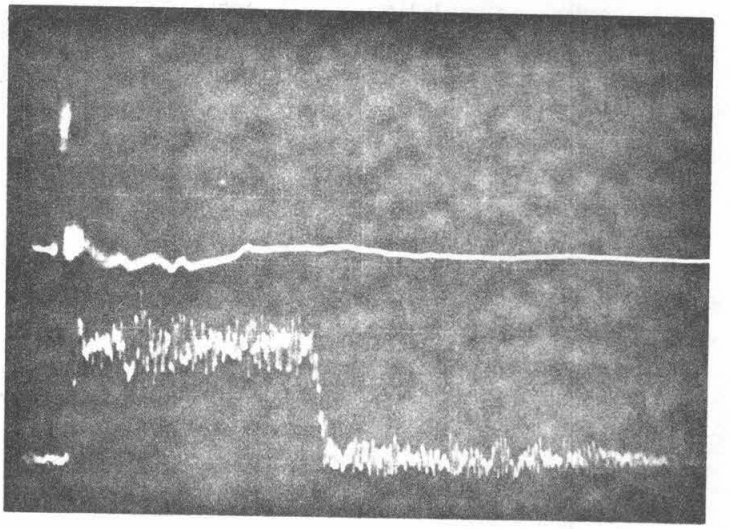

An example of a torsional stress pulse measured by strain gages on the cylindrical surface.

Scale: Vertical, 12.5×10^6 dyne/cm^2

Horizontal, 20 $\theta\mu$ sec/div -- upper beam
20 μ sec/div -- lower beam

FIGURE 3

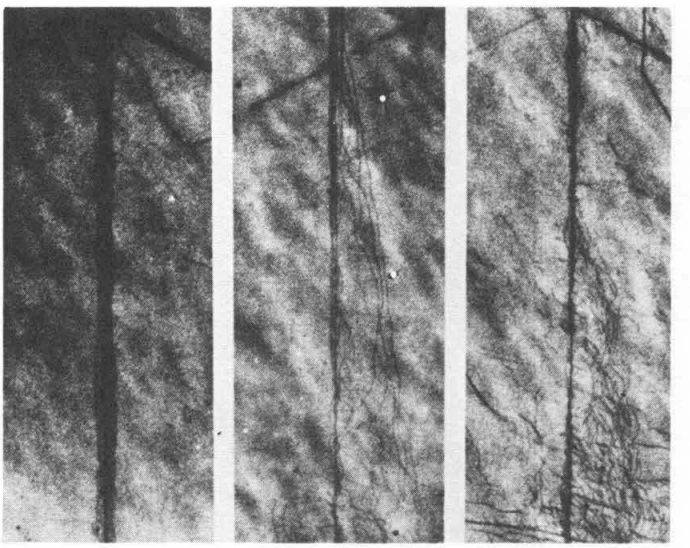

(a) (b) (c)

Berg-Barrett X-ray topographs for edge dislocation displacements (a) after scratching, ρ_f is about $10^5 cm^{-2}$, (b) after torsion test, ρ_f is about $10^2 cm^{-2}$, (c) after torsion test, ρ_f is $7 \times 10^4 cm^{-2}$. (Center of each specimen is at the top center of the picture.) (X 18.5)

FIGURE 4

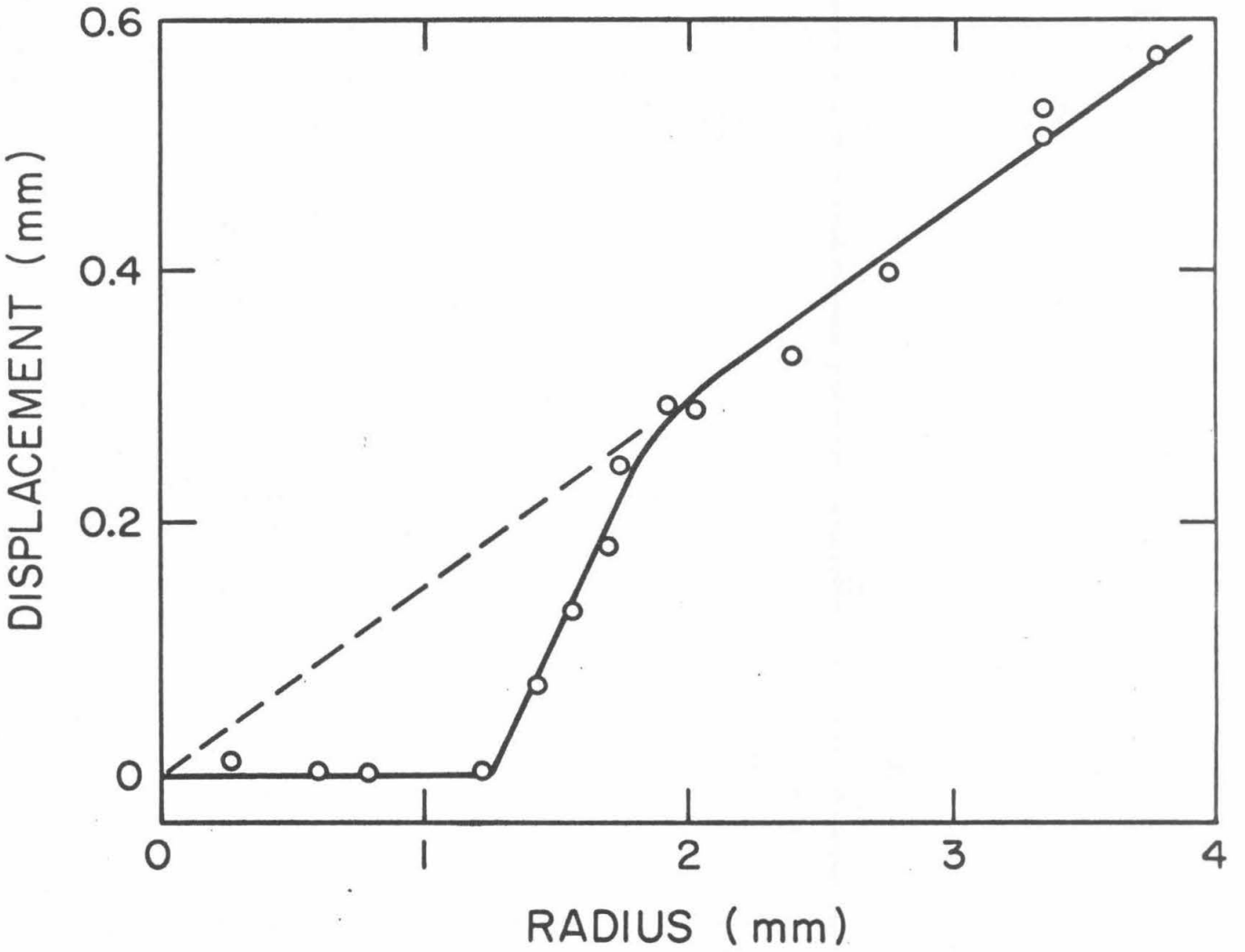

An example of edge dislocation displacements as a function of specimen radius obtained from Fig. 3(c).

FIGURE 5

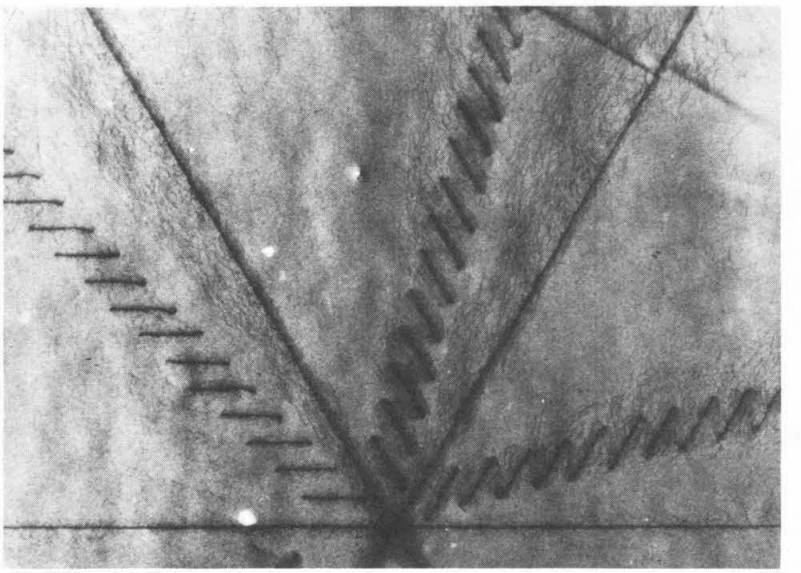

Berg-Barrett X-ray topograph for screw dislocation displacements. (Center of the specimen is at the bottom center of the figure.) (X 20.5)

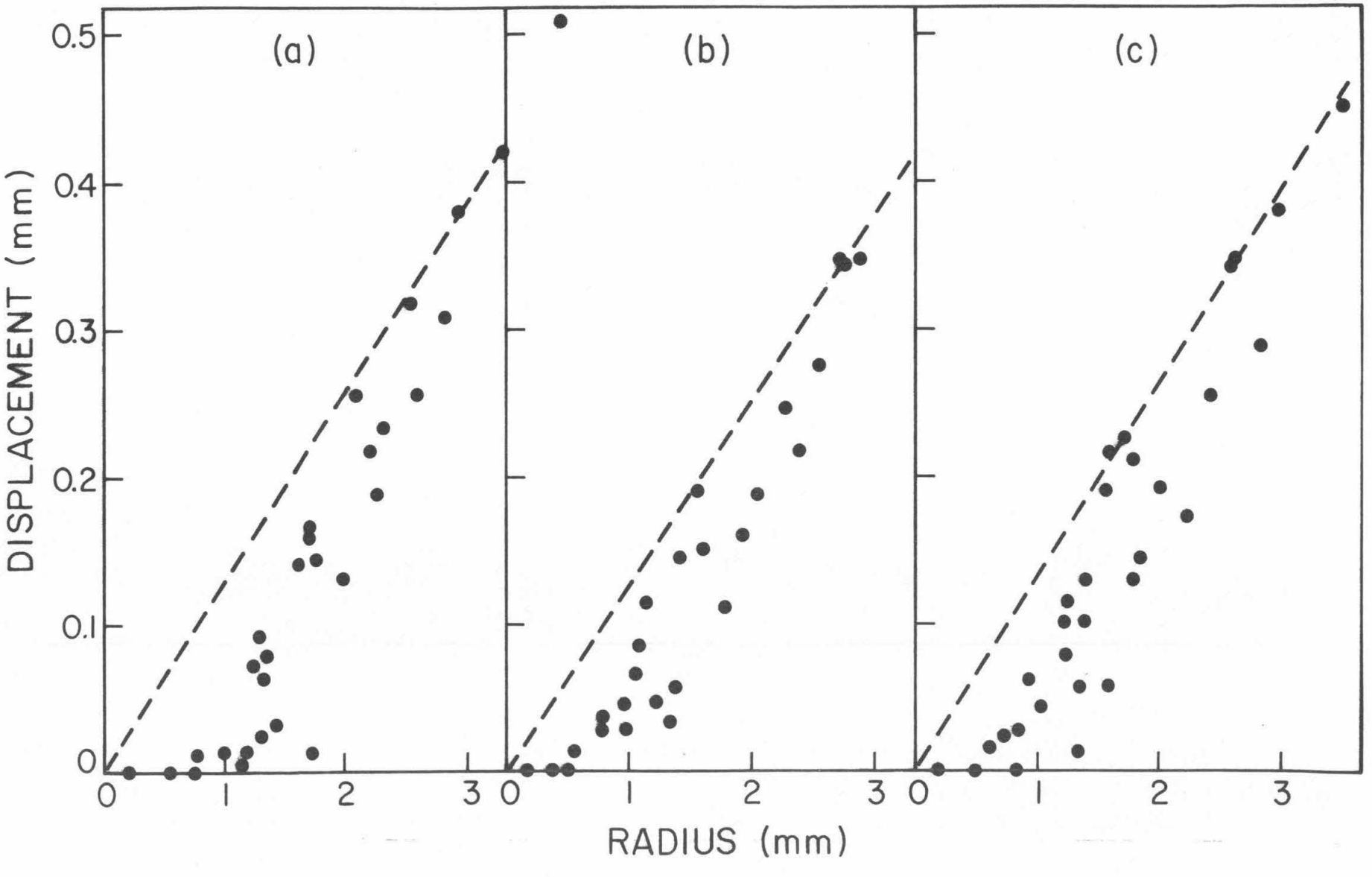

Screw dislocation displacements at room temperature as a function of specimen radius. (a) is for $\bar{a}_1$ basal dislocations and (b) and (c) are $\bar{a}_2$ or $\bar{a}_3$ dislocations.

FIGURE 6

TABLE I

Experimental Values of τ_c and βk for Edge Dislocations at Room Temperature

Interaction	Dislocation Density cm^{-2}	τ_c dyne/cm^2	$\beta k = \frac{\tau_c b}{2E\sqrt{\rho_f/2}}$
$\bar{a}_1 \pm (\bar{c} \pm \bar{a}_1)$	9.0×10^4	2.8×10^6	0.57
	1.8×10^5	3.6×10^6	0.52
	2.0×10^5	4.4×10^6	0.61
	4.0×10^5	6.2×10^6	0.60
	4.9×10^5	6.1×10^6	0.53
	7.6×10^5	8.2×10^6	0.57
a_2 or a_3 $\pm (\bar{c} \pm \bar{a}_1)$	6.6×10^4	1.9×10^6	0.45
	1.8×10^5	2.5×10^6	0.36
	2.0×10^5	3.1×10^6	0.42
	3.8×10^5	4.1×10^6	0.41
	4.2×10^5	3.5×10^6	0.33
	7.6×10^5	6.8×10^6	0.47
	7.6×10^5	7.3×10^6	0.51
	1.8×10^6	9.4×10^6	0.43
	1.8×10^6	1.1×10^7	0.51

TABLE 2

Comparison of Values of τ_c for Edge and Screw Dislocations at Different Temperatures

	Interaction	Temperature ^{o}K	Dislocation Density cm^{-2}	τ_c dyne/cm^2
Edge Dislocations	$\bar{a}_1 \pm (\bar{c} \pm \bar{a}_1)$	298	9.0×10^4	2.8×10^6
		84	9.7×10^4	2.7×10^6
	a_2 or $a_3 \pm (\bar{c} \pm \bar{a}_1)$	298	6.6×10^4	1.9×10^6
		84	6.3×10^4	1.9×10^6
Screw Dislocations	$\bar{a}_1 \pm (\bar{c} \pm \bar{a}_1)$	298	6.0×10^4	2.1×10^6
		84	1.0×10^5	4.1×10^6
	a_2 or $a_3 \pm (\bar{c} \pm \bar{a}_1)$	298	6.0×10^4	1.6×10^6
		84	9.0×10^4	2.7×10^6

TABLE 3

Comparison of Values of the Drag Coefficient B

Temperature ^{o}K	Dislocation Density cm^{-2}	Component	Burgers Vector	B from Present Results 10^{-4} dyne·sec/cm^2	B from Previous Results 10^{-4} dyne·sec/cm^2
298	7×10^4	edge	$\bar{a}_1$	3.2	3.5 (1)
			$\bar{a}_2$ or $\bar{a}_3$	3.2	
	6×10^4	screw	$\bar{a}_1$	3.5	3.4 (1)
			$\bar{a}_2$ or $\bar{a}_3$	3.5	
84	7×10^4	edge	$\bar{a}_1$	1.28	1.36 (2)
			$\bar{a}_2$ or $\bar{a}_3$	1.25	
	7×10^4	screw	$\bar{a}_1$	1.20	1.13 (3)
			$\bar{a}_2$ or $\bar{a}_3$	1.20	

(1) Pope and Vreeland (1969a) Forest dislocation densities were 10^3 to 10^4 cm^{-2}.

(2) Vreeland and Jassby (1971)

(3) This investigation, Forest density about 10^3 cm^{-2}.